Journal of Electronic Materials (2022) 51:1905–1921
https://doi.org/10.1007/s11664-022-09457-2

TOPICAL COLLECTION: SYNTHESIS AND ADVANCED CHARACTERIZATION OF MAGNETIC OXIDES

Magnetic Properties of a (1−x)$Bi_{0.5}Na_{0.5}TiO_3$+x$CaNiO_{3-\delta}$ Solid Solution System Prepared by Sol–Gel Technique

D. D. Dung[1] · N. H. Thoan[1] · N. Q. Dung[2] · P. V. Vinh[3] · N. H. Lam[1] · V. T. Lam[1] · P. D. Luong[1] · D. Q. Van[4]

Received: 19 October 2021 / Accepted: 17 January 2022 / Published online: 18 February 2022
© The Minerals, Metals & Materials Society 2022

Abstract

A new solid solution system of (1-*x*)$Bi_{0.5}Na_{0.5}TiO_3$+*x*$CaNiO_{3-\delta}$ compounds were synthesized by the sol–gel technique. The x-ray diffraction and Raman scattering structural studies indicated that the $CaNiO_{3-\delta}$ compound was well solid soluble in the host $Bi_{0.5}Na_{0.5}TiO_3$ crystals to form solid solutions. The random incorporation of Ca and Ni cations into the $Bi_{0.5}Na_{0.5}TiO_3$ host materials resulted in a distortion of lattice parameters, subsequently, in modification of the electronic band structure, and induced complex magnetic properties of the host materials. An enhancement of the magnetic properties of $Bi_{0.5}Na_{0.5}TiO_3$ materials resulted from complex-site preferences of *A*-sites via Ca cations together with transition Ni cations substituted for the *B*-site in the perovskite structures. Our results were essential to point out that the co-modification of both *A* and the *B*-sites via alkaline earth and transition metals, respectively, in lead-free ferroelectric $Bi_{0.5}Na_{0.5}TiO_3$ materials had opened a new method to improve magnetic performance for smart electronic applications.

Keywords $Bi_{0.5}Na_{0.5}TiO_3$ · $CaNiO_{3-\delta}$ · lead-free ferroelectric · ferromagnetism · sol–gel

Introduction

Lead-free ferroelectric $Bi_{0.5}Na_{0.5}TiO_3$ materials, which were first synthesized in the early 1960s by Smolenski et al.,[1,2] exhibit a large remnant polarization (P_r) and high Curie temperature (T_C) of P_r ~ 38 μC/cm^2 and T_C ~ 320 °C, respectively. However, because of high conductivity and a high coercive field (E_C), it is difficult to pole the materials by applying an external electrical field, resulting in a low piezoelectric coefficient (d_{33}) of 74–95 pC/N and dielectric constant (ε) of 425.[1–5] Therefore, the electrical performance of lead-free ferroelectric $Bi_{0.5}Na_{0.5}TiO_3$ materials is far lower than that of $Pb(Zr,Ti)O_3$-based (PZT-based) materials at this time.[1] Thus, the materials were undeveloped for a long time because of health and environmental protection concerns due to large quantities of toxic Pb element (~ 60 wt.%).[1,6] In the past, lead-free ferroelectric $Bi_{0.5}Na_{0.5}TiO_3$ materials attracted much research attention for development, such as via using dopants/solid solution method and/or by searching for active dopants with accordant concentrations of fabrication condition.[1,7–10] Recently, our review work pointed out that the electrical performance of $Bi_{0.5}Na_{0.5}TiO_3$-based materials was rapidly improved compared with PZT-based materials and started to be transferred to real applications.[1,11] Recently, the observation of room-temperature ferromagnetism in lead-free ferroelectric $Bi_{0.5}Na_{0.5}TiO_3$ material promised to extend functional materials for the next generation of electronic devices by using the biferroic property of one of the materials.[12,13] Both theoretical and experimental studies have suggested that the origin of ferromagnetic ordering in undoped lead-free ferroelectric $Bi_{0.5}Na_{0.5}TiO_3$ materials is mostly raised from Na and/or Ti vacancies.[12,14,15] However, the main problem is

✉ D. D. Dung
dung.dangduc@hust.edu.vn

✉ D. Q. Van
vandq@hnue.edu.vn

1 Multifunctional Ferroics Materials Lab, School of Engineering Physics, Ha Noi University of Science and Technology, 1 Dai Co Viet Road, Ha Noi, Vietnam

2 Department of Chemistry, Thai Nguyen University of Education, Thai Nguyen City, Vietnam

3 Faculty of Engineering Physics and Nanotechnology, VNU University of Engineering and Technology, 144 Xuan Thuy Road, Cau Giay district, Hanoi, Vietnam

4 Faculty of Physics, Hanoi National University of Education, 136 Xuan Thuy Road, Hanoi, Vietnam

that the magnetization of intrinsic $Bi_{0.5}Na_{0.5}TiO_3$ materials is low, only about ~ 1 memu/g at room temperature, and strongly influenced by the diamagnetic components of Ti^{4+} cations.[12,16] Therefore, improving the magnetic performance of lead-free ferroelectric $Bi_{0.5}Na_{0.5}TiO_3$-based materials is the next challenge for developing new functions in smart electronic devices. In fact, the simple method to inject the ferromagnetism into lead-free ferroelectric $Bi_{0.5}Na_{0.5}TiO_3$ materials is via using impurities such as transition metals (e.g., Fe, Co, Ni, Mn, and Cr).[16–22] Thanh et al.[15] pointed out that the magnetic properties of Cr-doped $Bi_{0.5}Na_{0.5}TiO_3$ materials were slightly enhanced due to the magnetic behavior of oxygen vacancies. In addition, Thanh et al.[17] reported that the magnetic properties of $Bi_{0.5}Na_{0.5}TiO_3$ materials were greatly enhanced by injecting Mn cations where the ferromagnetic order originated from the interaction of $Mn^{2+/3+}$ cations through oxygen vacancies (□), e.g., $Mn^{2+/3+}$-□-$Mn^{2+/3+}$. Wang et al.[18] and Dung et al.[19] also reported that the ferromagnetic exhibition at room temperature of Fe-doped $Bi_{0.5}Na_{0.5}TiO_3$ materials resulted from the interactions of Fe^{3+} cations through oxygen vacancies such as Fe^{3+}-□- Fe^{3+}, which were similar to the case of Mn-doped $Bi_{0.5}Na_{0.5}TiO_3$ materials. The results were also well consistent with the observation in Ni-doped $Bi_{0.5}Na_{0.5}TiO_3$ materials where the possible interactions of Ni cations through oxygen vacancies were favored for ferromagnetic order at room temperature, e.g., $Ni^{2+/3+}$-□- $Ni^{2+/3+}$.[20] However, unlike the case of Fe-, Mn-, Ni-, or Cr-doped $Bi_{0.5}Na_{0.5}TiO_3$ materials, the origin of ferromagnetic order at room temperature of Co-doped $Bi_{0.5}Na_{0.5}TiO_3$ materials was contrasted in recent reports.[21,22] Wang et al. [23] reported that the ferromagnetic at room temperature of Co-doped $Bi_{0.5}Na_{0.5}TiO_3$ materials originated from the magnetic behavior of Co clusters formed during hydrothermal synthesis, while Dung et al.[24] reported that the room-temperature ferromagnetism of Co-doped $Bi_{0.5}Na_{0.5}TiO_3$ materials might be raised from interactions of Co cations through oxygen vacancies such as $Co^{2+/3+}$-□-$Co^{2+/3+}$, as an intrinsic phenomenon. Interestingly, theoretical calculations of the electronic band structure for Fe-, Ni-, and Co-doped $Bi_{0.5}Na_{0.5}TiO_3$ materials showed that the possible charge transfers from transition metals to the empty state of the *d* orbital of Ti cations results in induced nonzero magnetic moments.[18,20,22] Even though the reports were not clear and even contrasted, the results were important to show that the magnetic moments of transition metal-doped $Bi_{0.5}Na_{0.5}TiO_3$ materials were greatly enhanced as expected in comparison with magnetic moments of pure $Bi_{0.5}Na_{0.5}TiO_3$ arising from self-defects.[12,16–22] Herein, the current issues are still debated, including (i) the origin of ferromagnetic order via interaction of transition metal cations randomly incorporated in host lattice, and (ii) the number limitation of the transition metals in the periodic table hindered the expansion in research since the strong influence of paramagnetic of isolated transition cations and/or antiferromagnetic coupling between magnetic polarons. Therefore, understanding the role of transition metal interaction to favor the magnetic order to control the magnetic moment and searching for a new method to inject the ferromagnetism into lead-free ferroelectric materials are important keys for the development of ferromagnetism based on lead-free ferroelectric materials.

The solid solution method is a new method for integrating ferromagnetic properties in lead-free ferroelectric $Bi_{0.5}Na_{0.5}TiO_3$ materials by selecting ilmenite-type (e.g., $MnTiO_3$, $NiTiO_3$, $CoTiO_3$, and $FeTiO_3$) and Fe-based perovskite-type (e.g., $SrFeO_{3-\delta}$, $MgFeO_{3-\delta}$, $CaFeO_{3-\delta}$, and $BaFeO_{3-\delta}$), Mn-based perovskite-type (e.g., $SrMnO_{3-\delta}$, $MgMnO_{3-\delta}$, $CaMnO_{3-\delta}$, or $BaMnO_{3-\delta}$), Co-based perovskite-type (e.g., $MgCoO_{3-\delta}$, $SrCoO_{3-\delta}$, $CaCoO_{3-\delta}$, and $BaCoO_{3-\delta}$) materials as impurities for solid solutions into host $Bi_{0.5}Na_{0.5}TiO_3$ materials.[15,23–36] The important results showed that the co-modification of ($Bi_{0.5}Na_{0.5}$) and Ti by alkaline earth and transition metals, respectively, enhanced the magnetic properties of the host $Bi_{0.5}Na_{0.5}TiO_3$ materials. In fact, the random distribution of alkaline-earth and transition metal co-modified lead-free ferroelectric $Bi_{0.5}Na_{0.5}TiO_3$ materials were complex modified magnetic properties of host $Bi_{0.5}Na_{0.5}TiO_3$ materials. The imbalance of alkaline-earth cations with Bi^{3+} and Na^{+} host cations of host $Bi_{0.5}Na_{0.5}TiO_3$ materials resulted in complex point defects in the host $Bi_{0.5}Na_{0.5}TiO_3$ materials. Oxygen vacancies were generated when alkaline-earth cations were substituted for Bi^{3+}-sites, while Na vacancies were created when alkaline-earth cations were incorporated with Na^{+}-sites. Both experimental observation and theoretical predictions have confirmed that Na vacancies directly induced nonzero magnetic moments.[12,32,33] Our recent theoretical study predicted that oxygen vacancies did not directly induce magnetic moments.[32] However, the oxygen vacancies promoted the reduction of the Ti valence state from Ti^{4+} to Ti^{3+}.[15] The appearance of Ti^{3+} lattice defects induced the ferromagnetism and Ti^{4+} vacancies.[32,33] Therefore, we expected that the co-modification of alkaline-earth cations and transition metals in lead-free ferroelectric $Bi_{0.5}Na_{0.5}TiO_3$ materials could exhibit larger magnetic moments than in the case of a single transition metal dopant.[16–36] Recently, Dung et al. obtained ferromagnetism at room temperature in Ni-doped $Bi_{0.5}Na_{0.5}TiO_3$ materials.[23] The complex magnetic properties were also reported for $NiTiO_3$-modified $Bi_{1/2}Na_{1/2}TiO_3$ and $Bi(Ti_{1/2}Ni_{1/2})O_3$-modified $Bi_{0.5}Na_{0.5}TiO_3$ materials.[23,24,37] However, so far, there is no report on the magnetic properties of alkaline-earth nickel-based perovskite $AeNiO_{3-\delta}$ solid solutions in lead-free ferroelectric $Bi_{0.5}Na_{0.5}TiO_3$ materials. Among alkaline-earth nickel-based perovskite $AeNiO_{3-\delta}$ family members (*Ae* = Ba, Ca, Sr, and Mg), $CaNiO_{3-\delta}$ is interesting because the O deficiency in three exiting

compounds of $CaNiO_3$, $CaNiO_2$, and $Ca_2Ni_2O_5$ (referred to as $CaNiO_{2.5}$) could be used to control the structural and magnetic properties.[38–40] Theoretical studies have predicted that $Ca_2Ni_2O_5$ and $CaNiO_3$ materials have an orthorhombic perovskite crystal structure, while $CaNiO_2$ has a tetragonal structure.[38–40] In addition, the theoretical using first-principles calculation predicted that the $CaNiO_2$ and $CaNiO_3$ materials exhibited zero magnetic moments, while $Ca_2Ni_2O_5$ have ferromagnetic behavior with a magnetic moment of 0.451 μ_B/f.u.[38–40]

So far, the solid solution between Ni-based perovskite-type materials has not been well reported. Among Ni-based nickelate perovskite-type materials, $CaNiO_{3-\delta}$ is not well reported as a solid solution in lead-free ferroelectric $Bi_{0.5}Na_{0.5}TiO_3$ materials. Therefore, we expected that by solid solution methods, Ca and Ni cations would randomly incorporate with the host $Bi_{0.5}Na_{0.5}TiO_3$ lattice, resulting in ferromagnetic order. In addition, the sol–gel method was used to flexibly control the chemical compositions.[15,23–37,41]

In this work, $CaNiO_{3-\delta}$-modified $Bi_{0.5}Na_{0.5}TiO_3$ materials were well synthesized by a simple sol–gel method. The lattice parameter distortion of $Bi_{0.5}Na_{0.5}TiO_3$ materials via solid solution $CaNiO_{3-\delta}$ materials resulted from the random distribution of Ca and Ni into the host lattices. The incorporation of Ca and Ni into the host $Bi_{0.5}Na_{0.5}TiO_3$ lattice exhibited a reduction of the optical bandgap and suppressed the photoluminescence. The complex magnetic properties of $Bi_{0.5}Na_{0.5}TiO_3$ materials were obtained as a function of $CaNiO_{3-\delta}$ concentration in the solid solutions.

Experimental

(1−*x*)$Bi_{0.5}Na_{0.5}TiO_3$+*x*$CaNiO_{3-\delta}$ (*x* = 0, 0.5, 1, 3, 5, 7, and 9 mol.%, designated as BNT pure and BNT-*x*$CaNiO_{3-\delta}$, respectively) were synthesized using a simple sol–gel technique. The starting materials were bismuth (III) nitrate pentahydrate ($Bi(NO_3)_3.5H_2O$, Sigma-Aldrich, 98%), sodium nitrate ($NaNO_3$, Sigma-Aldrich, 99.0%), calcium carbonate ($CaCO_3$, Sigma-Aldrich, ≥99.0%), nickel (II) nitrate hexahydrate ($Ni(NO_3)_2.6H_2O$, Sigma-Aldrich, 99.0%), and titanium (IV) isopropoxide ($C_{12}H_{28}O_4Ti$, Sigma-Aldrich, 98%). A selected chemical ligand was a mixing solution of acetic acid (CH_3COOH, Sigma-Aldrich, ≥ 99%) and acetylacetone ($CH_3COCH_2COCH_3$, Sigma-Aldrich, ≥99%) in deionized water with the volume ratio of 1:1:2. Firstly, raw $CaCO_3$ was weighed with the identified dopant concentration and dissolved in the former solution by magnetic stirring until transparent and without CO_2 bubbles. Secondly, $Bi(NO_3)_3.5H_2O$ was weighed and dissolved in the solution by continuous magnetic stirring. Subsequently, $NaNO_3$ and end-off $Ni(NO_3)_2.6H_2O$ were weighed and dissolved in the final solution. When the chemical solution was transparent, $C_{12}H_{28}O_4Ti$ was dropped into the solution to form the gel. The final solution was maintained under continuous magnetic stirring for about 3–5 h to form the homogeneous chemical solution. Thus, the dry gels were prepared by heating the gel in an oven at around 100–120°C. The dry gels were rout gridded before thermal annealing at around 800°C for 5 h in air to form powder samples. After thermal treatment, the samples were naturally cooled to room temperature. The powder samples were simply gridded before characterization of their properties. The chemical compositions were measured by energy-dispersive x-ray spectroscopy analysis (EDS, S-4800 Hitachi) and further confirmed by electron probe x-ray microanalysis (EPMA, Shimadzu EPMA 1600) measurements. Because Na cations could easily evaporate from the solution during drying and sintering processes, the Na source was weighed to an extra amount of 30–40 mol.%.[17–20,42] Crystal structures were confirmed by x-ray diffraction (XRD, Bruker D8 Advance) and Raman scattering (with a 473-nm LASOS laser and a DU420A-Oe defector) techniques. The influence of Ca and Ni on the optical properties of the host $Bi_{0.5}Na_{0.5}TiO_3$ materials was characterized by ultraviolet–visible (UV–Vis, Jasco V-670) spectroscopy and photoluminescence (PL, exciter with 473-nm LASOS laser and a DU420A-Oe defector) spectra. Magnetic properties of (1-*x*)$Bi_{0.5}Na_{0.5}TiO_3$+*x*$CaNiO_{3-\delta}$ compounds were investigated by a vibrating sample magnetometer (VSM, Lakeshore 7404). All measurements were performed at room temperature.

Results and discussion

The evidence for the presence of chemical elements in pure and $CaNiO_{3-\delta}$-modified $Bi_{0.5}Na_{0.5}TiO_3$ materials are shown in Fig. 1a and b, respectively. The EDS spectra in Fig. 1a and b confirm the presence of the constituent elements, including Bi, Na, Ti, and O in the pure BNT sample, and Bi, Na, Ti, O, Ca, and Ni in the 5-mol.%-$CaNiO_{3-\delta}$-modified BNT sample, respectively. The EDS spectrum of the pure $Bi_{0.5}Na_{0.5}TiO_3$ material, shown in Fig. 1a, confirmed the presence of all expected elements, including Bi, Na, Ti, and O. Two additional typical peaks for Ca and Ni elements are observed in the EDS spectrum of 5 mol.% $CaNiO_{3-\delta}$-modified $Bi_{0.5}Na_{0.5}TiO_3$ material, presenting solid evidence of the existence of Ca and Ni impurity elements in the host $Bi_{0.5}Na_{0.5}TiO_3$ compounds.

The homogeneous distribution of Ca and Ni impurity elements of $CaNiO_{3-\delta}$-modified $Bi_{0.5}Na_{0.5}TiO_3$ samples with 5 mol.% of $CaNiO_{3-\delta}$ is proved in Fig. 2. Figure 2a and b show a selected area for chemical mapping and the final chemical mapping of all elements, respectively. The element mappings of host elements, including Bi, Na, Ti, O, and impurity elements of Ni and Ca, are shown in Fig. 2c–h, respectively.

The results pointed out that both host and impurity elements were homogeneously distributed in our studied samples.

The roles of Ca and Ni cations in the $Bi_{0.5}Na_{0.5}TiO_3$ host lattices were studied by XRD measurements, as shown in Fig. 3a for pure $Bi_{0.5}Na_{0.5}TiO_3$ and $CaNiO_{3-\delta}$-modified $Bi_{0.5}Na_{0.5}TiO_3$ samples with various $CaNiO_{3-\delta}$ concentrations. Based on the peak positions and their relative intensity, the crystal structure of $Bi_{0.5}Na_{0.5}TiO_3$ materials was indexed as a rhombohedral structure (JCPDS card no. 00-036-0340, space group R3c). This result was consistent with recent observation on the crystal symmetry of $Bi_{0.5}Na_{0.5}TiO_3$ materials synthesized by the sol–gel method.[17–20,42] The addition of $CaNiO_{3-\delta}$ with concentration up to 9 mol.% into host $Bi_{0.5}Na_{0.5}TiO_3$ materials did not change the crystal structure of host $Bi_{0.5}Na_{0.5}TiO_3$ materials, where no extra peaks of impurity phase and/or phase separation were observed under the resolution of the XRD method. This important result pointed out that $CaNiO_{3-\delta}$ was well dissolved into the host $Bi_{0.5}Na_{0.5}TiO_3$ materials to form solid solutions. Furthermore, the roles of Ca and Ni cations randomly incorporated with the $Bi_{0.5}Na_{0.5}TiO_3$ host lattices during the formation of solid solutions are shown in Fig. 3b, where the XRD patterns are magnified in the 2θ range from 31.0° to 34.0°, showing the overlapping of (012)/(110) double peaks due to rhombohedral symmetry. The (012)/(110) satellite peaks were distinguished by Lorentzian fitting with *r*-square values over 0.99. Based on the results of fitting XRD for pure and $CaNiO_{3-\delta}$-modified $Bi_{0.5}Na_{0.5}TiO_3$ samples, the peak position was complexly distorted as a function of $CaNiO_{3-\delta}$ concentrations. Furthermore, the lattice parameters *a* and *c* of the pure $Bi_{0.5}Na_{0.5}TiO_3$ and the $CaNiO_{3-\delta}$-modified $Bi_{0.5}Na_{0.5}TiO_3$ according to $CaNiO_{3-\delta}$ addition amounts are shown in Fig. 3c. The results show that distorted lattice parameters of $Bi_{0.5}Na_{0.5}TiO_3$ compound are not linear as a function of $CaNiO_{3-\delta}$ amounts that have complex distortion in lattice parameters. This could be attributed to the radius difference between impurity Ca and Ni cations and Bi, Na, and Ti cations of the host materials. The complex distortion of lattice parameters was possibly explained by the radius difference between impurity (Ca or Ni) cations with host cations, such as Bi/Na cations at *A*-sites and/or Ti cations

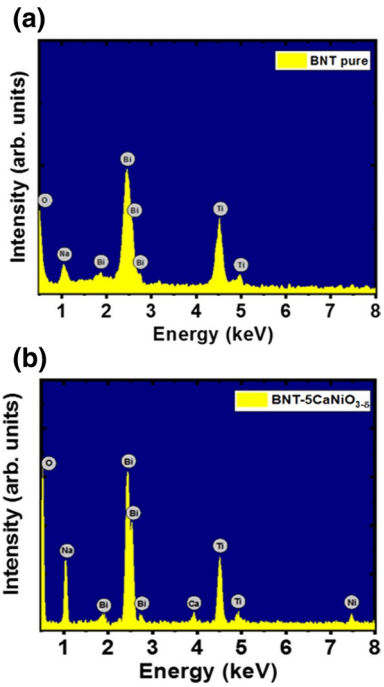

Fig. 1 EDS spectral for (a) the pure $Bi_{0.5}Na_{0.5}TiO_3$ and (b) 5 mol.% $CaNiO_{3-\delta}$-modified $Bi_{0.5}Na_{0.5}TiO_3$ solid solution.

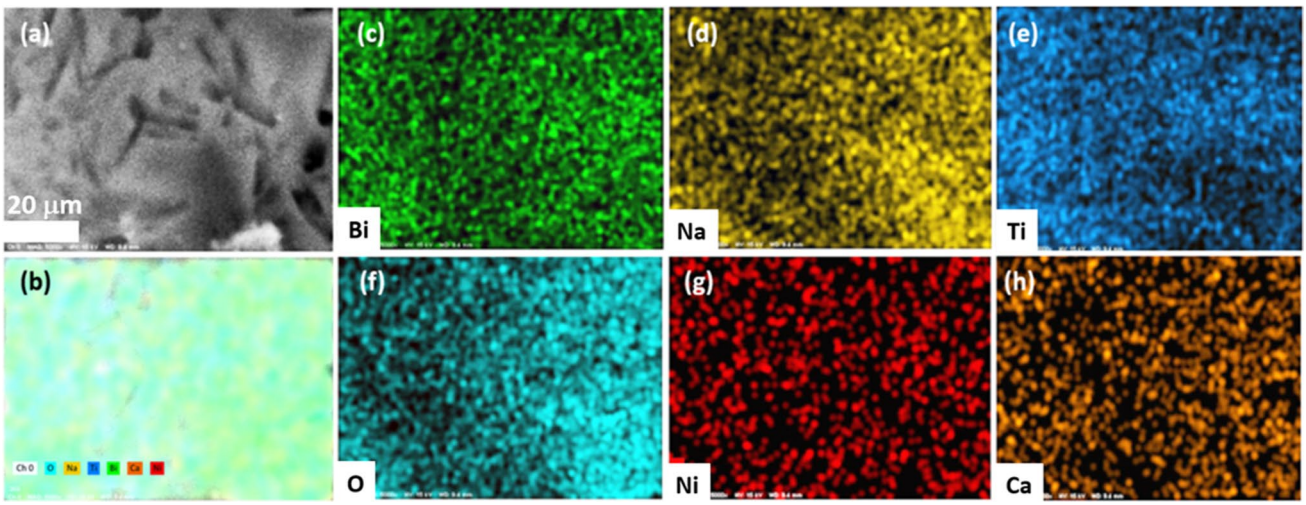

Fig. 2 Chemical mapping for 5 mol.% $CaNiO_{3-\delta}$-modified $Bi_{0.5}Na_{0.5}TiO_3$ solid solution: (a) the selected area for EDS mapping, (b) the total contribution of all elements, (c–h) separation of chemical mapping for Bi, Na, Ti, O, Ni, and Ca, respectively.

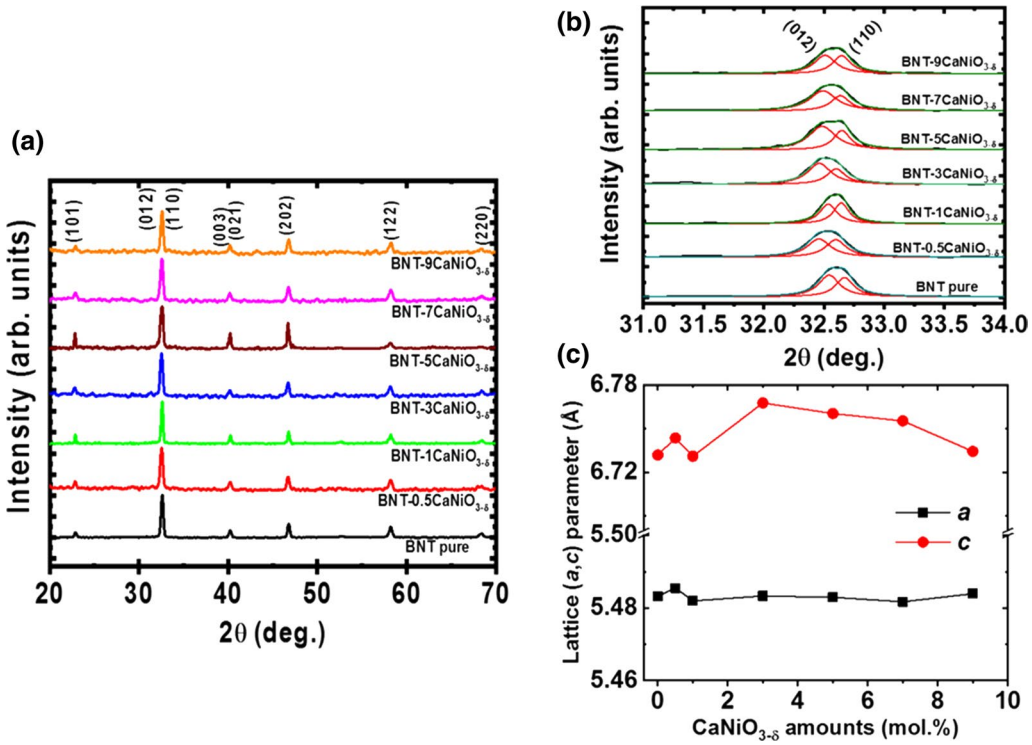

Fig. 3 (a) X-ray diffraction patterns and (b) convolution satellite (012)/(110) peaks in the 2θ range from 31.0° to 34.0° of the pure $Bi_{0.5}Na_{0.5}TiO_3$ and $CaNiO_{3-\delta}$-modified $Bi_{0.5}Na_{0.5}TiO_3$ solid solutions with various $CaNiO_{3-\delta}$ concentrations, and (c) lattice constants of the pure $Bi_{0.5}Na_{0.5}TiO_3$ and $CaNiO_{3-\delta}$-modified $Bi_{0.5}Na_{0.5}TiO_3$ solid solutions at 0.5, 1, 3, 5, 7, and 9 mol.% of $CaNiO_{3-\delta}$.

at *B*-sites of $Bi_{0.5}Na_{0.5}TiO_3$ materials. The radius of Bi^{3+} cations (in the coordination number of VIII), Na^+ cations (in the coordination number of XII), and Ti^{4+} cations (in the coordination number of VI) are 1.17, 1.39, and 0.605 Å, respectively.[43] The radius of Ca^{2+} cations (in the coordination number of XII) is 1.34 Å which is about 14.5% larger than that of Bi^{3+} cations and 3.6% smaller than that of Na^+ cations.[43] Therefore, the substitution of Ca^{2+} cations for Na-sites would result in compressing lattice parameters; otherwise, the lattice parameter was expanded when Ca^{2+} was incorporated with Bi- or Ti-sites in the host lattices. However, unlike Ca cations, Ni cations exhibited various radius values, which strongly depended on their valence and spin states.[43] At the coordination number of VI, the Ni^{2+} cations have a radius of 0.690 Å, while Ni^{3+} cation low-spin (LS) and high-spin (HS) states have radii of 0.56 Å and 0.60 Å, respectively.[43] The Ni^{4+} cations have only exhibited at LS state with a radius of 0.48 Å.[43] Thus, lattice parameters of the host $Bi_{0.5}Na_{0.5}TiO_3$ materials would be expanded if Ni^{2+} or HS-state Ni^{3+} cations were incorporated with Ti^{4+} cations at *B*-sites, while the compressor lattice parameter was dominant when the Ni cations were stable at Ni^{3+} (for LS state) and Ni^{4+} (for LS state). The Ni cations were recently reported to exhibit various valence states when they are randomly incorporated with the host lattices of $Bi_{0.5}Na_{0.5}TiO_3$-based materials.[20,24,37,44] At this time, the direct evidence of Ni concentration effects on the valence and spin states is unclear in current research; therefore, it is hard to point out the main reason for distortion lattice parameters which were contributed by Ni cations substituted at the Ti-site. The origin of the lattice parameter distortion of the host $Bi_{0.5}Na_{0.5}TiO_3$ materials became more complex when the random Ca cations were incorporated with a specific *A*-site, which is consistent. The imbalance of valence states between Ca^{2+} impurity cations and the host cations Bi^{3+} and Na^+ resulted in complex results. Oxygen vacancies were created when Ca^{2+} cations were incorporated with the Bi^{3+}-site, and Na^+ vacancies were generated when Ca^{2+} cations were substituted for the Na^+-site. In addition, the number of oxygen vacancies was also increased because of the substitution of low-valence states $Ni^{2+/3+}$ for Ti^{4+}-sites. Note that the size of oxygen vacancies of 1.31 Å was smaller than the size of the oxygen anion of 1.4 Å.[45] Na non-stoichiometry also induced the distortion of lattice parameters.[4,5,46–48] Moreover, the enhancement of oxygen vacancy concentration bonding around Ti^{4+} cations promoted the reduction of the valence state to Ti^{3+}, resulting in expansion of the lattice parameter.[15,49] Note that the radius of Ti^{3+} cations (in the coordination number of VI) are 0.670 Å, which is larger than that of Ti^{4+} cations of 0.605 Å with the same

coordination number.[43] Thus, the main origin of the lattice parameter distortion of the host $Bi_{0.5}Na_{0.5}TiO_3$ materials was complex where the various parameters were possibly co-effective via the random incorporation of Ca and Ni cations into the host lattice. However, the lattice parameter distortion as a function of $CaNiO_{3-\delta}$ amounts was direct evidence for the random incorporation of Ca and Ni cations during solid solution formation. In other words, the $Bi_{0.5}Na_{0.5}TiO_3$ materials effectively carried the impurity $CaNiO_{3-\delta}$ phase as solid solutions.

Figure 4a presents the Raman scattering spectra of the pure $Bi_{0.5}Na_{0.5}TiO_3$ and $CaNiO_{3-\delta}$-modified $Bi_{0.5}Na_{0.5}TiO_3$ materials as a function of $CaNiO_{3-\delta}$ concentrations, showing the influence of Ca and Ni cations on the vibration phonon modes of the host $Bi_{0.5}Na_{0.5}TiO_3$ crystal. The broadband in Raman spectra was obtained for all studied samples, possibly resulting from a random arrangement of Bi and Na cations at the *A*-site in the perovskite structure.[50] However, the Raman spectra of all samples could be divided into three overlapping regions. Similar shapes were obtained for the pure and $CaNiO_{3-\delta}$-modified $Bi_{0.5}Na_{0.5}TiO_3$ samples, providing evidence for the remaining structure of $Bi_{0.5}Na_{0.5}TiO_3$ materials. The results were consistent with the observation of the maintained structure of the pure $Bi_{0.5}Na_{0.5}TiO_3$ materials with $CaNiO_{3-\delta}$-added $Bi_{0.5}Na_{0.5}TiO_3$ up to 9 mol.%, as predicted by XRD measurement. The Raman scattering peaks were possibly obtained using a fitting function with approximately Lorentzian with *r*-square over 0.99. The results of the approximately fitting contribution of hidden Raman peaks for pure and $CaNiO_{3-\delta}$-modified $Bi_{0.5}Na_{0.5}TiO_3$ materials are shown in Fig. 4b. The peak positions were well matched which theoretical prediction and experimental observation.[29–31,50] However, the intensity of possible Raman scattering peaks was dependent on the $CaNiO_{3-\delta}$ amounts in the solid solutions. The reduction of the Raman intensity was possibly related to the destroy of the crystal symmetry of pure $Bi_{0.5}Na_{0.5}TiO_3$ materials due to random incorporation of Ca and Ni cations into host lattice. In addition, the distortion of vibration modes around 583 cm^{-1} to high frequencies with increasing $CaNiO_{3-\delta}$ amount was suggested for incorporation of Ni into Ti due to the heavier mass of Ni cations (~58.71 g/mol) in comparison with the mole mass of Ti cations (~ 47.90 g/mol). The shift of high-frequency Raman peaks was recently reported for transition metals (e.g., Mn, Co, Fe, or Ni) substituted for Ti at *B*-sites in the perovskite structure of $Bi_{0.5}Na_{0.5}TiO_3$ materials.[24–31] The XRD and Raman scattering studies showed that the $CaNiO_{3-\delta}$ materials were well solid soluble into the host $Bi_{0.5}Na_{0.5}TiO_3$ materials.

The random incorporation of Ca and Ni cations into the host lattice of $Bi_{0.5}Na_{0.5}TiO_3$ during the formation of a solid solution resulted in modification of the electronic band structure of the host $Bi_{0.5}Na_{0.5}TiO_3$ materials. The absorption spectrum of pure $Bi_{0.5}Na_{0.5}TiO_3$ materials and $CaNiO_{3-\delta}$-modified $Bi_{0.5}Na_{0.5}TiO_3$ materials as a function of $CaNiO_{3-\delta}$ are plotted in Fig. 5a. The absorption spectrum of pure $Bi_{0.5}Na_{0.5}TiO_3$ materials showed a single absorption edge with a slight tail, which resulted from self-defect and/or was related to surface defects.[15] The presence of self-defect such as O or Na vacancies or Ti^{3+} defects was recently detected by x-ray photoelectron spectroscopy.[15] The modification of the electronic structure of $Bi_{0.5}Na_{0.5}TiO_3$ materials via using $CaNiO_{3-\delta}$ as a solid solution was shown by two important observations of the absorption spectroscopy: (i) the shift of the absorption edge to the high-absorption photon wavelength and (ii) the appearance of new broad emission via absorption spectroscopy. The shift of the absorption edge was suggested to relate to the appearance

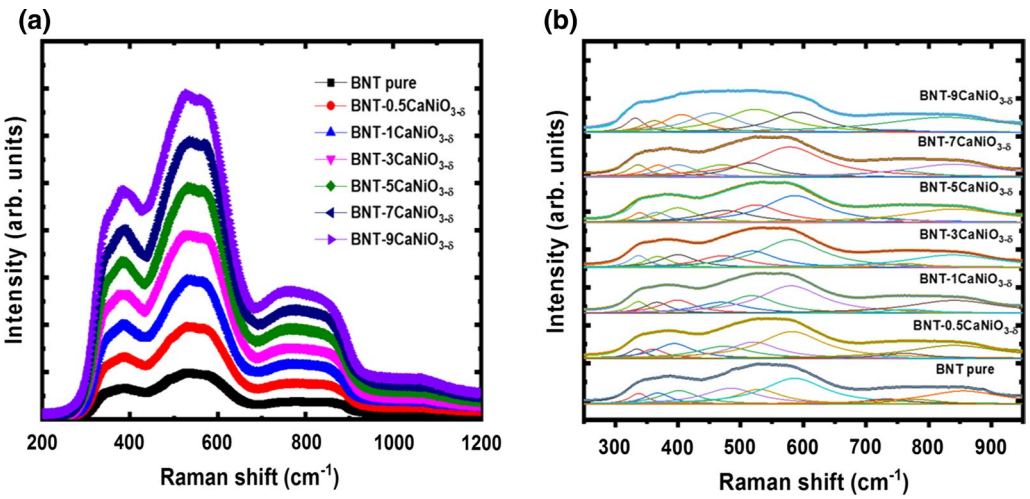

Fig. 4 (a) Raman scattering spectra and (b) the deconvolution of the pure $Bi_{0.5}Na_{0.5}TiO_3$ and $CaNiO_{3-\delta}$-modified $Bi_{0.5}Na_{0.5}TiO_3$ solid solutions.

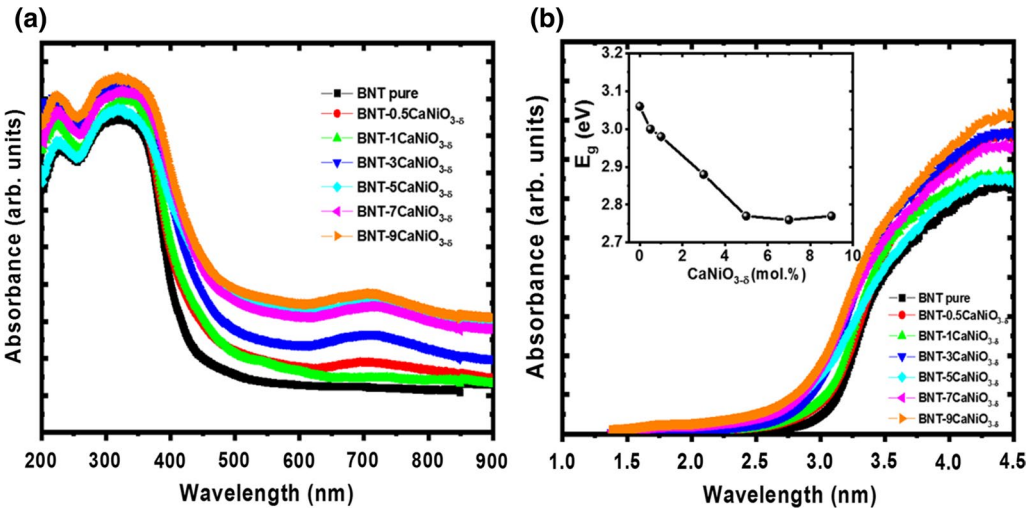

Fig. 5 (a) Absorption spectra and (b) the $(\alpha h\gamma)^2$ as a function of absorption photon energy ($h\gamma$) of pure $Bi_{0.5}Na_{0.5}TiO_3$ and $CaNiO_{3-\delta}$-modified $Bi_{0.5}Na_{0.5}TiO_3$ materials with various $CaNiO_{3-\delta}$ concentrations as solid solutions. The inset of Fig. 5b shows the dependence of effective optical bandgap as a function of $CaNiO_{3-\delta}$ concentration.

of new local states in the electronic band structure, such as the levels of Ni defects and Ca defects, which were consistent with recently reported in $CaFeO_{3-\delta}$-modified $Bi_{0.5}Na_{0.5}TiO_3$ materials.[32] The appearance of new broad emission in the absorption spectra of $Bi_{0.5}Na_{0.5}TiO_3$ materials with increasing $CaNiO_{3-\delta}$ concentration was suggested to originate from electron transfer between the inner 3*d* level of Ni cations.[20,24,37] Moreover, the appearance of vacancy states such as Na or O vacancies and/or Ti^{3+} defects was also possible given the new local state in the electronic band structure, which resulted in a reduction of the effective optical bandgap. Recently, Linh et al. predicted the electronic band structure of $Bi_{0.5}Na_{0.5}TiO_3$ compound, that the $Bi_{0.5}Na_{0.5}TiO_3$ materials have a direct bandgap transition.[51] Thus, the optical bandgaps of pure $Bi_{0.5}Na_{0.5}TiO_3$ and $CaNiO_{3-\delta}$-modified $Bi_{0.5}Na_{0.5}TiO_3$ materials were estimated by the Wood–Tauc method,[15,18] where the $(\alpha h\gamma)^2$ values were plotted as a function of absorption photon energy ($h\gamma$). Figure 5b shows the proportion of $(\alpha h\gamma)^2$ values as a function of absorption ($h\gamma$) for pure and $CaNiO_{3-\delta}$-modified $Bi_{0.5}Na_{0.5}TiO_3$ materials. Thus, the optical bandgap (E_g) values were roughly obtained from fitting curves. The dependence of E_g values is shown in the inset of Fig. 5b. The estimation of E_g values for pure $Bi_{0.5}Na_{0.5}TiO_3$ materials was around 3.07 eV, consistent with recent reports for optical bandgap values of pure $Bi_{0.5}Na_{0.5}TiO_3$ materials which were synthesized by a sol–gel route.[15,18] The results indicated that the optical bandgap values of pure $Bi_{0.5}Na_{0.5}TiO_3$ materials tended to reduce to 2.75 eV with $CaNiO_{3-\delta}$ increasing up to 7 mol.% in the $CaNiO_{3-\delta}$ solute solution in $Bi_{0.5}Na_{0.5}TiO_3$ materials and slightly increased with further addition of $CaNiO_{3-\delta}$ up to 9 mol.%. The reduction of optical bandgap in $CaNiO_{3-\delta}$-modified $Bi_{0.5}Na_{0.5}TiO_3$ materials was quite complex compared to single Ni-doped $Bi_{0.5}Na_{0.5}TiO_3$ materials where the optical bandgap of Ni-doped $Bi_{0.5}Na_{0.5}TiO_3$ materials decreases monotonically as a function of Ni dopant concentration.[20] The role of Ni impurities in the electronic band structure of $Bi_{0.5}Na_{0.5}TiO_3$ materials was recently reported experimentally and was quite consistent with the first-principles theoretical prediction that the Ni cations induced a new local state in the middle bandgap.[20] However, the random incorporation of Ca cations with *A*-site (Bi, and Na) was quite complex, where the Ca substitution for

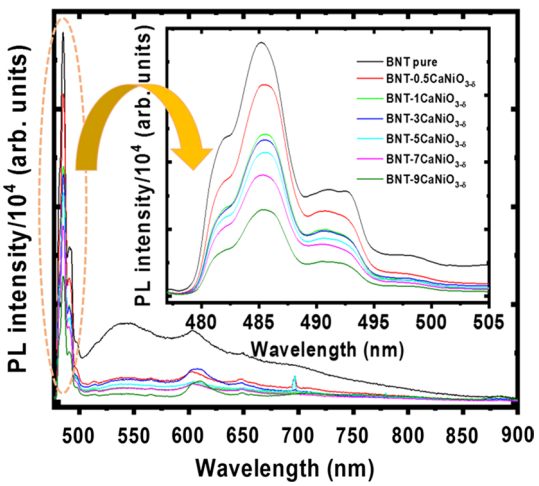

Fig. 6 PL spectra of the pure $Bi_{0.5}Na_{0.5}TiO_3$ and $CaNiO_{3-\delta}$-modified $Bi_{0.5}Na_{0.5}TiO_3$ with various $CaNiO_{3-\delta}$ concentrations as solid solutions. The inset of Fig. 3 shows the magnification of PL spectra in the photon wavelength range from 478 mm to 505 nm.

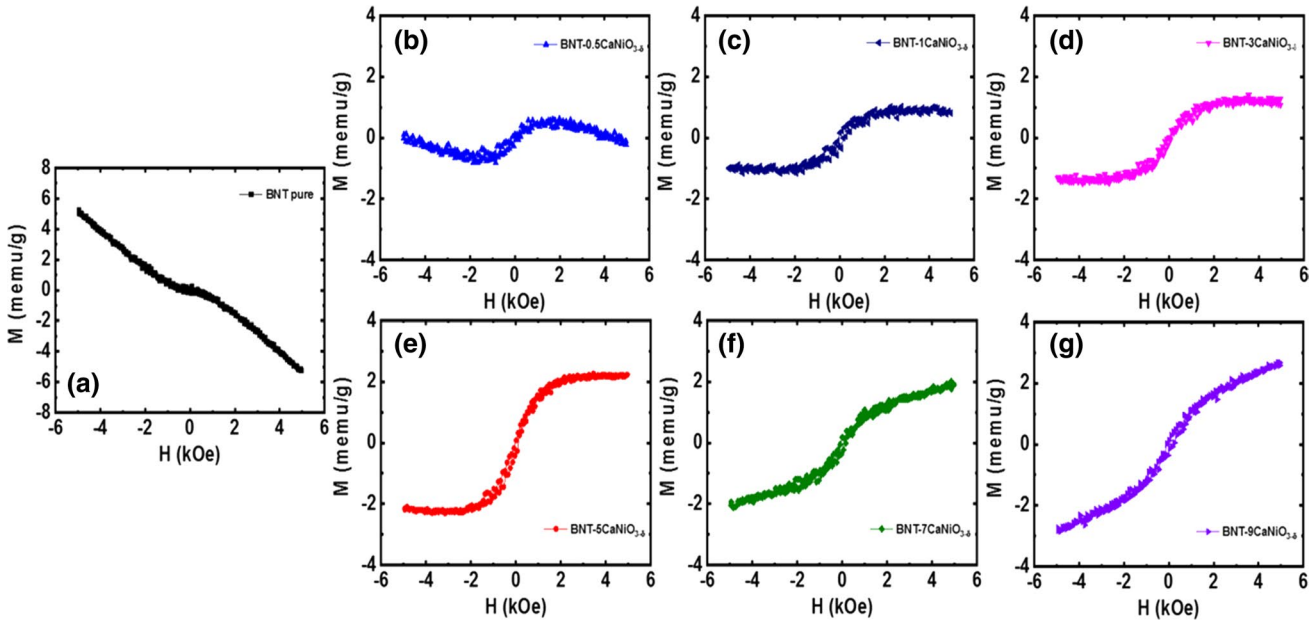

Fig. 7 M-H curves of (a) pure $Bi_{0.5}Na_{0.5}TiO_3$ materials and $CaNiO_{3-\delta}$-modified $Bi_{0.5}Na_{0.5}TiO_3$ materials with $CaNiO_{3-\delta}$ amounts of (b) 0.5 mol.%, (c) 1 mol.%, (d) 3 mol.%, (e) 5 mol.%, (f) 7 mol.%, and (g) 9 mol.%.

Bi-sites results in the generation of oxygen vacancies where Ca cations incorporated for Na-sites created Na vacancies.[32] The vacancies could trap a photon or make a charge transfer, which could affect the effective optical bandgap of the pure $Bi_{0.5}Na_{0.5}TiO_3$ materials. However, the optical bandgap values were slightly reduced by increasing the $CaNiO_{3-\delta}$ concentration up to 7 mol.% and increased again for 9 mol.% $CaNiO_{3-\delta}$. The complex trend in the optical bandgap of the $CaNiO_{3-\delta}$-modified $Bi_{0.5}Na_{0.5}TiO_3$ materials was possibly explained by various effects that could co-contribute. First, the appearance of new local defects such as Ni and Ca defects could reduce the effective optical bandgap. Second, the appearance of vacancies, e.g., oxygen vacancies, generated from valance-state imbalance of $Ni^{2+/3+}$ and Ti^{4+} or Ca^{2+} and Bi^{3+}, could also reduce the optical bandgap.[51] The complex distortion of lattice parameters due to random incorporation of Ca cations at *A*-sites and Ni cations at *B*-sites also influenced the electronic structure, leading to a change in the optical bandgap.[52] Moreover, the oxygen vacancies promoted a change in the valence state of Ti^{4+} to $Ti^{3+,}$ which also affected the electronic band structure of $Bi_{0.5}Na_{0.5}TiO_3$ materials with new defect states.[32,49] In addition, due to the limitation of XRD and Raman scattering, the possibility of clusters or phase denegation of Ni-rich phase existed, and/or Ni cations were possibly located at the interstitial, resulting in a contrasting trend in the optical bandgap. However, the dependence of the optical bandgap of $Bi_{0.5}Na_{0.5}TiO_3$ materials on the $CaNiO_3$ contents was solid evidence for the incorporation of Ca and Ni into host lattice $Bi_{0.5}Na_{0.5}TiO_3$ crystal.

The influence of $CaNiO_{3-\delta}$ concentrations on the photoluminescence (PL) of $Bi_{0.5}Na_{0.5}TiO_3$ materials is shown in Fig. 6. The PL of $Bi_{0.5}Na_{0.5}TiO_3$ materials exhibited a broad band, where strong PL was recorded in the range

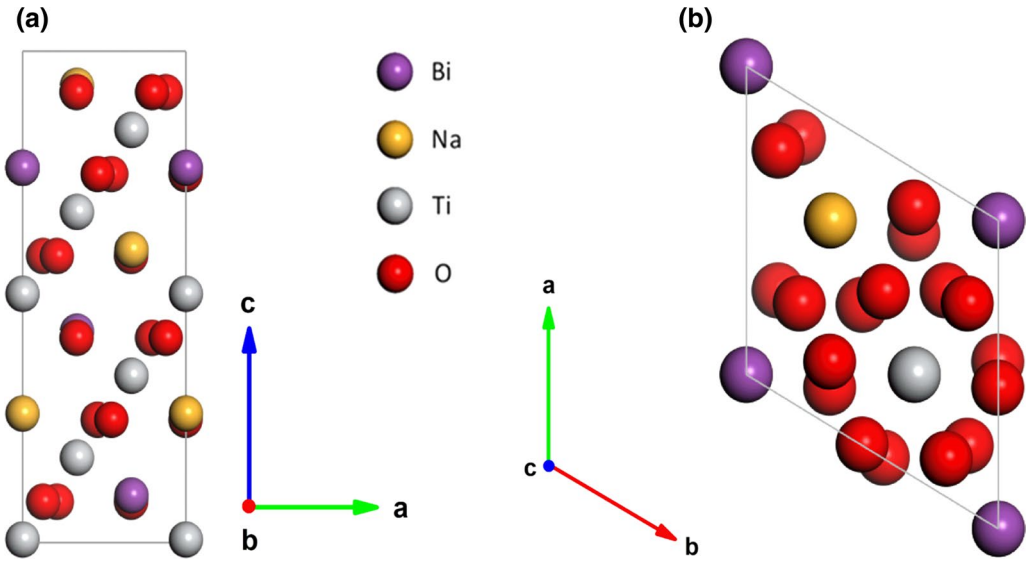

Fig. 8 (a, b) Side and top views of the optimized atomic structures of intrinsic $Bi_{0.5}Na_{0.5}TiO_3$ (BNT).

of 480–500 nm. Pure $Bi_{0.5}Na_{0.5}TiO_3$ materials exhibited strong PL around 485 nm. Thus, we suggested that the main PL peaks were not assigned to band-to-band transitions. So far, the original peaks in the PL results of pure $Bi_{0.5}Na_{0.5}TiO_3$ materials are still unclear. Unlike oxide materials, $Bi_{0.5}Na_{0.5}TiO_3$ materials are ferroelectric. Therefore, their materials are constructed from the natural ferroelectric domain. The polarization of the electrical domains prevented electron–hole recombination from generating new photons. Note that the recombination of electron–hole pairs is basically for the PL mechanism. Recently, the PL behavior of pure $Bi_{0.5}Na_{0.5}TiO_3$ materials was explained by surface defects where the atoms at the surface had fewer pair bonds than atoms inside the $Bi_{0.5}Na_{0.5}TiO_3$ materials.[32,53] Herein, we noted that the origin of PL peaks still needs further investigation. The addition of $CaNiO_{3-\delta}$ into the host $Bi_{0.5}Na_{0.5}TiO_3$ materials as solid solutions resulted in suppression of PL intensity. The magnified PL spectra as a function of $CaNiO_{3-\delta}$ concentrations are shown in the inset of Fig. 6 in the wavelength range of 478−505 nm. The results indicated that the PL intensity of the $Bi_{0.5}Na_{0.5}TiO_3$ materials was reduced by increasing $CaNiO_{3-\delta}$ concentrations. Suppression of the PL intensity of $Bi_{0.5}Na_{0.5}TiO_3$ materials was suggested for the photon absorption by trapping impurity cations and/or vacancies.[15] The suppression of PL intensity was well reported for lead-free ferroelectric $Bi_{0.5}Na_{0.5}TiO_3$ materials when solid-solute with various ABO_3-type materials.[15,28–30] We suggested that photons generated by Ti cations at the surface were trapped by the nearest Ni defects.

Room-temperature magnetic properties of the $Bi_{0.5}Na_{0.5}TiO_3$ materials as a function of $CaNiO_{3-\delta}$ concentrations are shown in Fig. 7a–g. The figures present complex shapes of M-H curves, indicating the complex magnetic properties of the system. The M-H curve of the pure $Bi_{0.5}Na_{0.5}TiO_3$ exhibited an anti-*S* shape, which was recently explained by the combination of the Ti^{4+} cation's diamagnetic property and self-defects.[12,15,16,32] Thanh et al. suggested that oxygen vacancies possibly

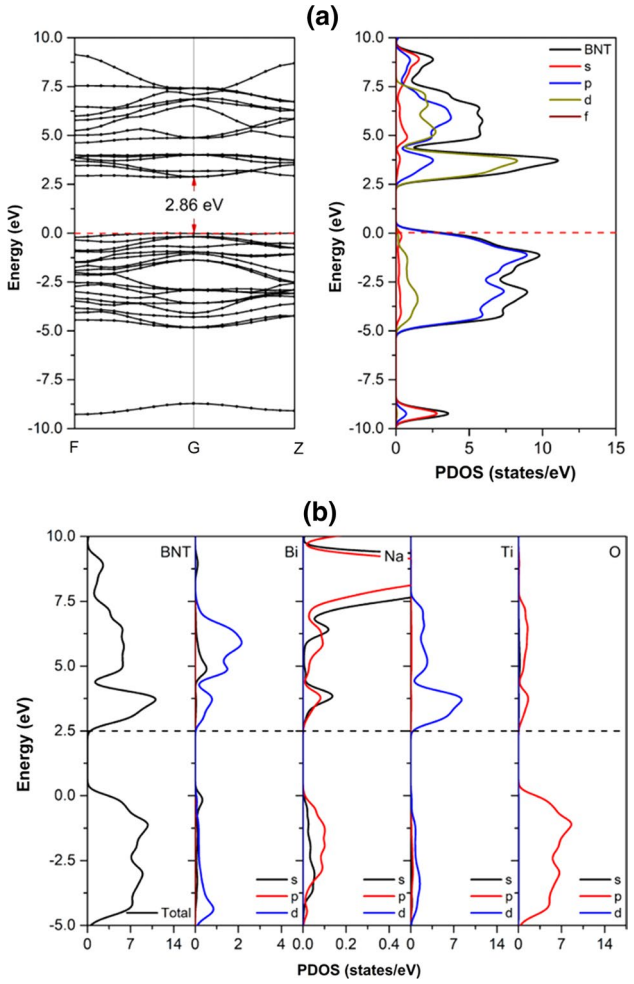

Fig. 9 The DFT results of (a) the band structures and partial density of states (PDOS) of BNT, (b) the contribution of each element in the formation of the total density of states (TDOS) of BNT. The Fermi level is set to zero energy.

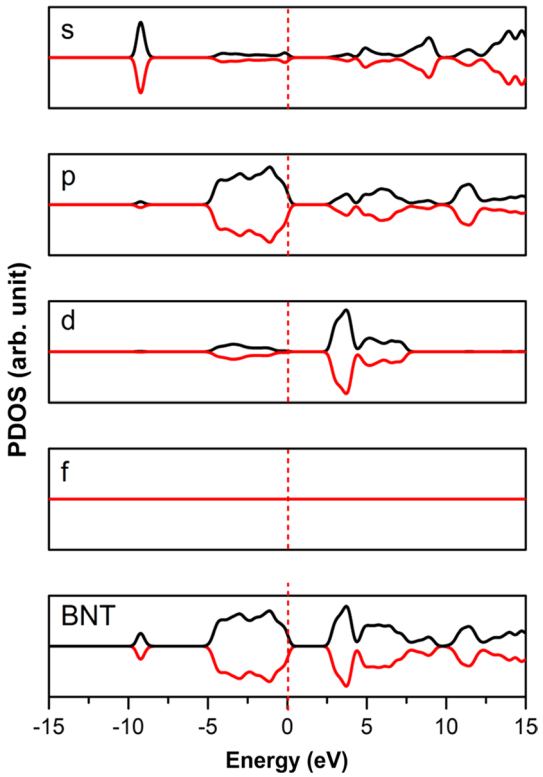

Fig. 10 The DFT results of the orbital projected density of states (PDOS) of BNT. The black and red lines represent the majority and minority spin states. The Fermi level is set to zero energy.

originated weak ferromagnetism at room temperature.[15] Ju et al. showed evidence for observations of ferromagnetic ordering at room temperature via controlling Na vacancies.[12] Recently, from both theoretical and experimental studies, the origin of room-temperature ferromagnetism in pure $Bi_{0.5}Na_{0.5}TiO_3$ compounds was ascribed to contributions of vacancies (e.g., Na, Ti, Bi vacancies) and Ti^{3+} defects.[16,32] The magnetic remanence (M_r) and coercive field (H_C) values of the $CaNiO_{3-\delta}$-modified $Bi_{0.5}Na_{0.5}TiO_3$ materials were obtained in the range of 0.21–0.11 memu/g and 94–146 Oe, respectively, consistent with recently reported values for transition metal-doped Bi-based or Pb-based materials.[54] The nonzero M_r and H_C values of the $CaNiO_{3-\delta}$ addition to $Bi_{0.5}Na_{0.5}TiO_3$ materials were solid evidence for ferromagnetic ordering at room

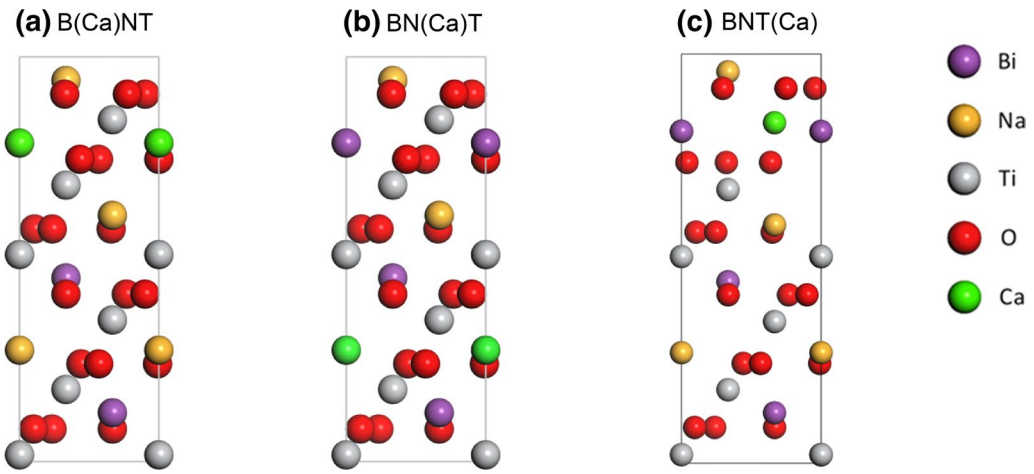

Fig. 11 Side views of the optimized atomic structures of the (a) Bi-site [B(Ca)NT], (b) Na-site [BN(Ca)T], and (c) Ti-site [BNT(Ca)] substituted BNT. The atomic symbols are indicated at the right of the figure.

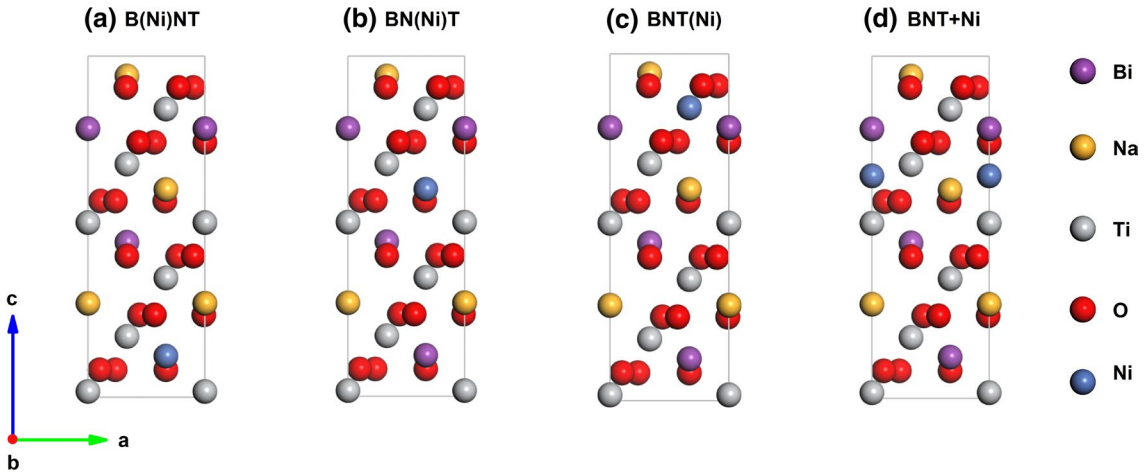

Fig. 12 Side views of the optimized atomic structures of the (a) Bi-site [B(Ni)NT], (b) Na-site [BN(Bi)T], (c) Ti-site [BNT(Ni)], and (d) interstitial [BNT+Ni] substituted BNT. The atomic symbols are indicated at the right of the figure.

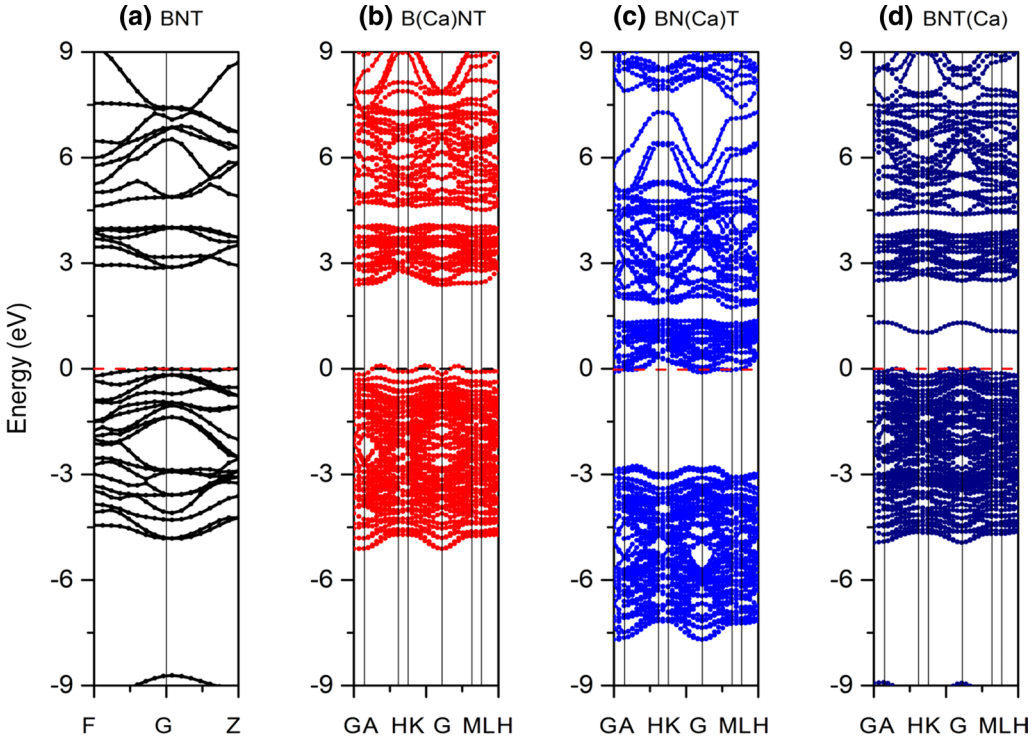

Fig. 13 The DFT results of the band structures of (a) BNT, (b) B(Ca)NT, (c) BN(Ca)T, and (d) BNT(Ca). The Fermi level is set to zero energy.

temperature. However, the addition of $CaNiO_{3-\delta}$ into the host $Bi_{0.5}Na_{0.5}TiO_3$ materials resulted in complex magnetic behavior which is strongly dependent on $CaNiO_{3-\delta}$ amounts, as shown in Fig. 7b–g. The slight addition with 0.5 and 1 mol.% of $CaNiO_{3-\delta}$ into the host $Bi_{0.5}Na_{0.5}TiO_3$ materials suppressed the diamagnetic component and induced the ferromagnetic components, as shown in S-shaped M-H curves in Fig. 7b and c, respectively. Figure 7d and e show that the magnetic moment as a function of the applied external magnetic field tended to saturate for the samples with 3 and 5 mol.% of $CaNiO_{3-\delta}$. When continuously adding $CaNiO_{3-\delta}$ up to 9 mol.%, the magnetic moments tended to be unsaturated with the applied external magnetic field. The slight addition of $CaNiO_{3-\delta}$ into the host $Bi_{0.5}Na_{0.5}TiO_3$ materials induced the interaction of Ni cations through oxygen vacancies which were possibly favored for ferromagnetic ordering, as proposed by Coey et al.[55] for *F*-center interaction of magnetic ions in oxide materials. Among the three valence states of Ni cation in nature, Ni^{4+} cations are stable at a low spin state only, while Ni^{2+} and Ni^{3+} possibly can exist in two spin states.[43] Recently, theoretical and experimental studies suggested that Ni cations are more favorable to stability with a low-spin state.[20] Therefore, it was suggested that the low magnetic moments in the $CaNiO_{3-\delta}$-modified $Bi_{0.5}Na_{0.5}TiO_3$ system would be due to the interactions of Ni cations with a low-spin state through oxygen vacancies.

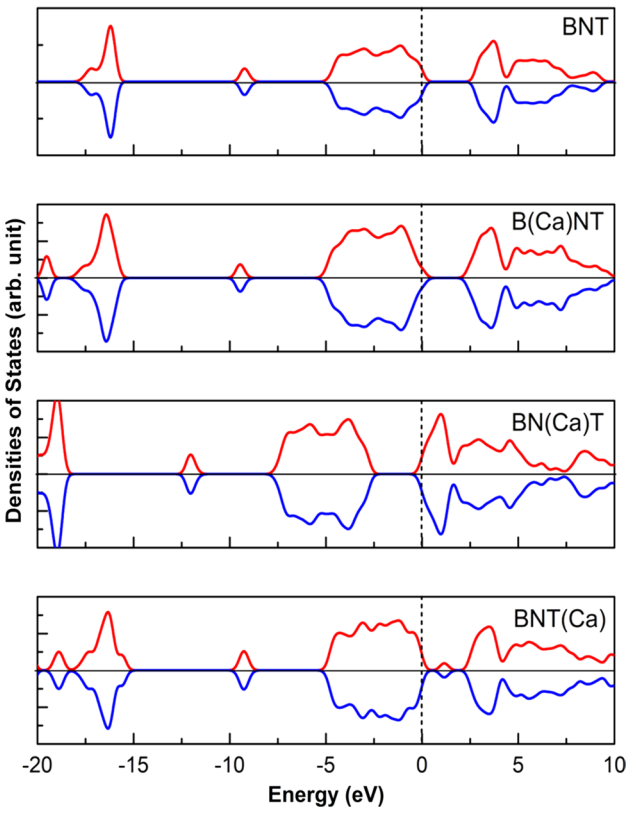

Fig. 14 The DFT results of the spin-resolved total density of states (TDOS) of BNT, B(Ca)NT, BN(Ca)T, and BNT(Ca). The Fermi level is set to zero energy.

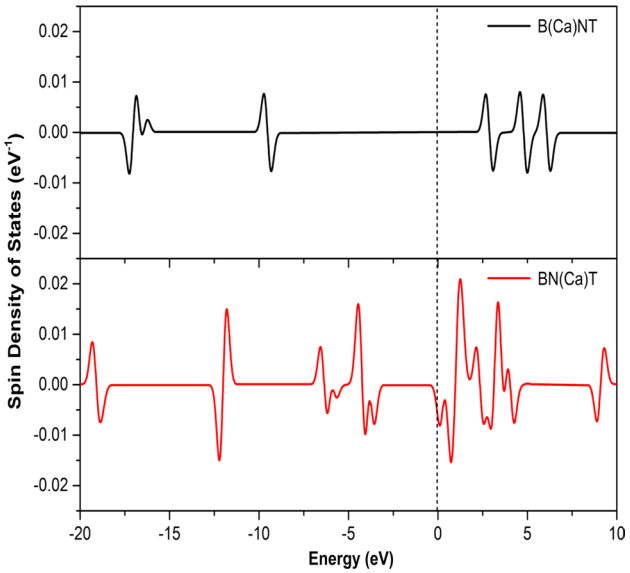

Fig. 15 The DFT results of the spin density of states of B(Ca)NT (upper) and BN(Ca)T (lower). The Fermi level is set to zero energy.

Moreover, another possible magnetism source was induced via Ti^{4+} vacancies or self-defects of $Ti^{2+/3+}$.[32] In fact, the magnetism of $CaNiO_{3-\delta}$-modified $Bi_{0.5}Na_{0.5}TiO_3$ system was complex because of possible multi-incorporation of Ca cations at *A*-sites in the host lattice of $Bi_{0.5}Na_{0.5}TiO_3$ materials, where the complex of a possible defect type was created.[32] The observation of ferromagnetism in lead-free ferroelectric $Bi_{0.5}Na_{0.5}TiO_3$ materials should be further investigated. In other words, the complex magnetic properties were obtained in the $CaNiO_{3-\delta}$-modified $Bi_{0.5}Na_{0.5}TiO_3$ system as a function of $CaNiO_{3-\delta}$ concentrations because of the co-modification of *A* and *B*-sites with alkaline earths and transition metals, respectively.

To explain the magnetic properties of $Bi_{0.5}Na_{0.5}TiO_3$ (BNT) modified by $CaNiO_{3-\delta}$, ab initio calculations were performed using the CASTEP module in the Materials Studio software.[56] The generalized gradient approximation (GGA) formulated by Perdew, Burke, and Ernzerhof (PBE) was used to describe the electron exchange-correlation potential.[57] An energy cutoff of 410 eV for the

Table I Integrated spin density of B(Ca)NT, BN(Ca)T, and BNT(Ca)

	B(Ca)NT	BN(Ca)T	BNT(Ca)
Integrated spin density $\left(\frac{\hbar}{2}\right)$	0.95×10^{-3}	-0.25×10^{-3}	-0.15×10^{-12}
Integrated |spin density| $\left(\frac{\hbar}{2}\right)$	0.50×10^{-2}	0.14×10^{-1}	0.74×10^{-3}
Magnetic behavior	Ferromagnetic	Ferrimagnetic	Ferrimagnetic

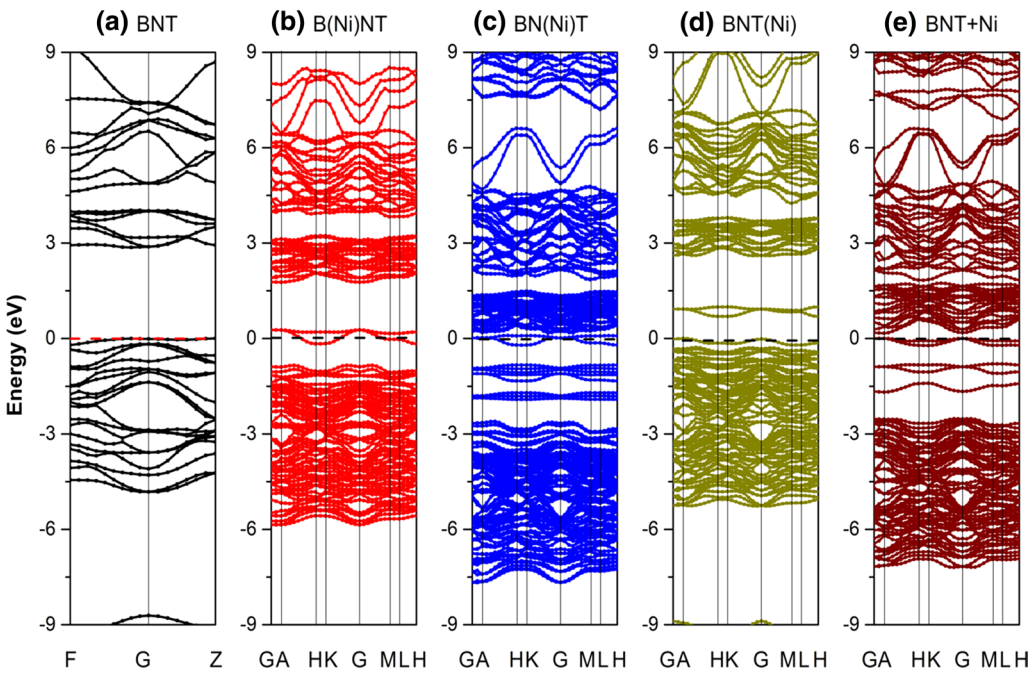

Fig. 16 The DFT results of the band structures of (a) BNT, (b) B(Ni)NT, (c) BN(Ni)T, (d) BNT(Ni), and (e) BNT+Ni. The Fermi level is set to zero energy.

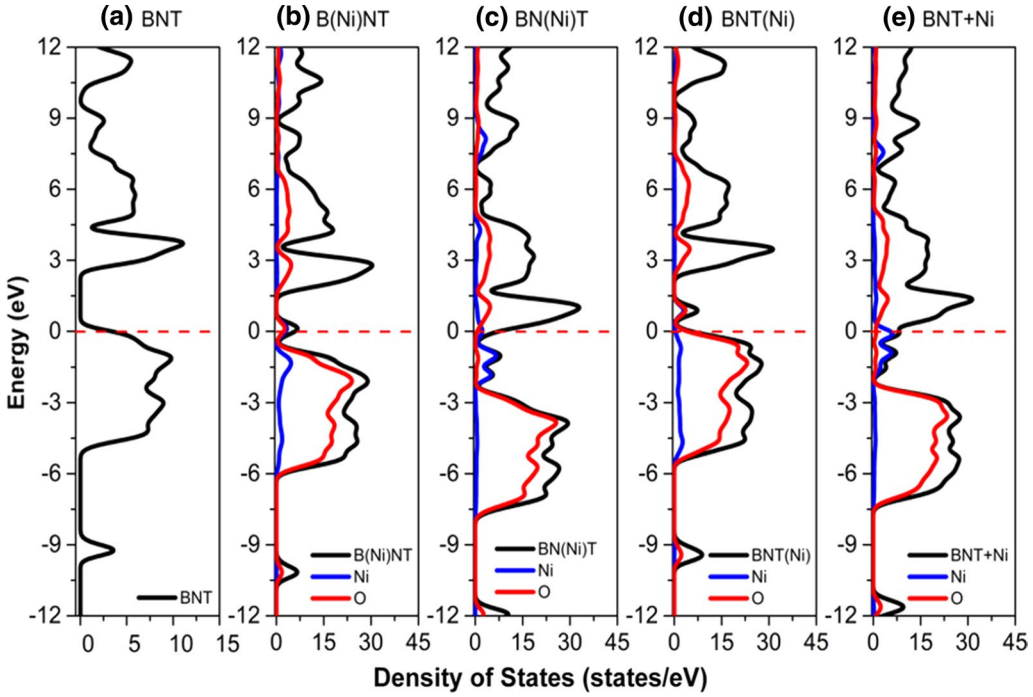

Fig. 17 The DFT results of the orbital projected density of states (PDOS) for (a) BNT, (b) B(Ni)NT, (c) BN(Ni)T, (d) BNT(Ni), and (e) BNT+Ni. The blue and red represent the Ni and O states, respectively. The Fermi level is set to zero energy.

plane-wave basis and a *k*-point mesh of 5 × 5 × 2 for the Brillouin zone integration were set for all calculations.[58] The optimization process stops when the change in the total energy between two ionic relaxation steps is less than 5×10^{-6} eV.

Figure 8a, b illustrate the hexagonal representation of a unit cell of intrinsic BNT with lattice parameters $a = b = 5.4939$ Å and $c = 13.8345$ Å, and containing three Bi atoms, three Na atoms, six Ti atoms, and 18 O atoms. The calculated electronic structures of the pure BNT in Fig. 9a indicate that BNT is a 2.86-eV direct-bandgap semiconductor, close to the experimental value of 3.07 eV. Using density functional theory (DFT) calculation of perovskite structures, one often gets estimated E_g values smaller than experimental values.[59] The partial density of states (PDOS) of BNT indicate that the valence and conduction bands are dominated by the 2*p* and 3*d* orbital states of O and Ti, respectively. Figure 10 shows that all the orbital majority and minority spin states of intrinsic BNT were entirely degenerated, suggesting that BNT is a nonmagnetic material, in good agreement with previous calculation.[32,33,60]

The effects of $CaNiO_{3-\delta}$ on the host material BNT are simply investigated by substituting Ca and Ni atoms into the host lattice. The *A*-site doping model was created by replacing one Bi or Na atom with one Ca/Ni atom, denoted as B(Ca/Ni)NT and BN(Ca/Ni)T, respectively. The *B*-site doping model was formed by introducing one Ca/Ni atom to replace one Ti atom, denoted as BNT(Ca/Ni), all illustrated in Figs. 11a–c and 12a–c, respectively. An extra model of interstitial doping into BNT lattice was built for the Ni atom, denoted as BNT+Ni, as shown in Fig. 12d.

Figure 13 presents the band structures of BNT, B(Ca)NT, BN(Ca)T, and BNT(Ca) models, calculated using the CASTEP package. For the B(Ca)NT model, the Fermi level is located just above the valence band, and this can be referred to as a *p*-type semiconductor, originating from the deficit of electrons in the unit cell. The scarcity of electrons originated from the valence difference between Bi^{3+} and Ca^{2+} ions. In contrast, the Fermi level in BN(Ca)T shifts upward and touches the conduction band bottom, suggesting that BN(Ca)T behaves as an *n*-doped semiconductor. The bandgap values of B(Ca)NT, BN(Ca)T, and BNT(Ca) are 2.30 eV, 2.65 eV, and 1.22 eV, respectively, smaller than

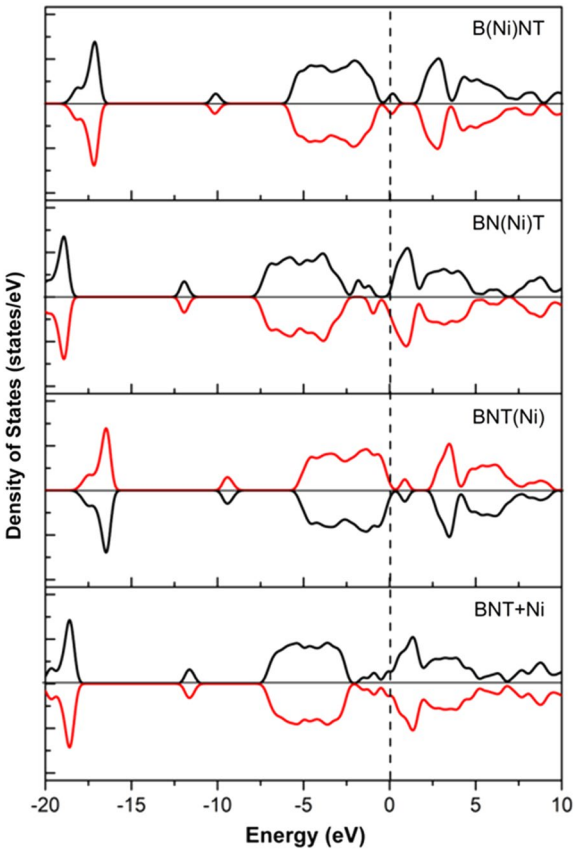

Fig. 18 The DFT results of the spin-resolved total density of states (TDOS) of B(Ni)NT, BN(Ni)T, BNT(Ni), and BNT+Ni. The Fermi level is set to zero energy.

that of intrinsic BNT, and in agreement with their DOS in Fig. 14.

Figure 14 presents the spin-resolved DOS of BNT, B(Ca)NT, BN(Ca)T, and BNT(Ca) in the range of −20 eV to 10 eV. It can be seen that all majority and minority spin states of all four models are completely degenerated, suggesting that the intrinsic and Ca-doped BNT are nonmagnetic materials. However, the spin DOS of B(Ca)NT and BN(Ca)T in Fig. 15 suggest that these models exhibit weak magnetic properties with a small magnetic moment per unit cell, in good agreement with integrated spin densities of B(Ca)NT, BN(Ca)T, and BNT(Ca) in Table I.[61]

Figure 16b–d illustrate the band structure of B(Ni)NT, BN(Ni)T, BNT(Ni), and BNT+Ni models, respectively. The Ni dopant gives rise to new midgap states in all four band structures and reduces the bandgap, in agreement with the partial density of states in Fig. 17. The PDOS in Fig. 17 also indicates that the hybridization of Ni and O atoms leads to the formation of these new midgap states. For the B(Ni)NT and BNT(Ni), the Fermi levels shift to the top of the valence bands, opposite of BN(Ni)T and BNT+Ni in which the Fermi level lies just below the conduction bands. This means that B(Ni)NT and BNT(Ni) are *p*-type semiconductors, and BN(Ni)T and BNT+Ni behave as *n*-type semiconductors.

Figure 18 presents the spin-resolved densities of states of B(Ni)NT, BN(Ni)T, BNT(Ni), and BNT+Ni in the range of −20 eV to 10 eV. The clear asymmetry of the majority and minority spin states in the range of −5 eV to 5 eV suggests that B(Ni)NT and BN(Ni)T are strong magnetic materials, opposite of BNT(Ni) and BNT+Ni, which may only exhibit weak magnetic properties, in good agreement with integrated spin densities of Ni-doped BNT models in Table II. The results in Table II also indicate that B(Ni)NT and BN(Ni)T exhibit ferromagnetic properties, whereas BNT(Ni) and BNT+Ni are ferrimagnetic materials.[61]

Conclusion

The complex $CaNiO_{3-\delta}$-modified $Bi_{0.5}Na_{0.5}TiO_3$ system was well synthesized by the sol–gel method. The Ca and Ni cations were found to be well incorporated with the host of $Bi_{0.5}Na_{0.5}TiO_3$ crystal, resulting in distortion of the lattice structure. The random influence of Ca and Ni cations in the host lattice of $Bi_{0.5}Na_{0.5}TiO_3$ materials displayed a reduction of optical bandgap and induced complex magnetic properties as a function of $CaNiO_{3-\delta}$ amounts. Controlling the optical and magnetic properties of lead-free ferroelectric $Bi_{0.5}Na_{0.5}TiO_3$ materials promises to extend the function of the material for application in smart electronic devices.

Table II Integrated spin density of B(Ni)NT, BN(Ni)T, BNT(Ni), and BNT+Ni

	B(Ni)NT	BN(Ni)T	BNT(Ni)	BNT+Ni
Integrated spin density $\left(\frac{\hbar}{2}\right)$	0.12×10^{-2}	1.00	-0.39×10^{-5}	-0.27×10^{-4}
Integrated |spin density| $\left(\frac{\hbar}{2}\right)$	0.18×10^{-2}	1.80	0.32×10^{-3}	0.36×10^{-3}
Magnetic behavior	Ferromagnetic	Ferromagnetic	Ferrimagnetic	Ferrimagnetic

Acknowledgments This research is funded by Vietnam National Foundation for Science and Technology Development (NAFOSTED) under grant number 103.02-2019.366.

Conflict of interest On behalf of all authors, the corresponding author states that there is no conflict of interest.

References

1. N.D. Quan, L.H. Bac, D.V. Thiet, V.N. Hung, and D.D. Dung, Current development in lead-free $Bi_{0.5}(Na, K)_{0.5}TiO_3$-based piezoelectric materials. *Adv. Mater. Sci. Eng.* 2014, 365391 (2014).
2. G.A. Smolensky, V.A. Isupov, A.I. Agranovskaya, and N.N. Krainic, New ferroelectrics with complex compounds. *Fiz. Tverd. Tela* 2, 2982 (1960).
3. M. Naderer, T. Kainz, D. Schutz, and K. Reichmann, The influence of Ti-nonstoichiometry in $Bi_{0.5}Na_{0.5}TiO_3$. *J. Eur. Ceram. Soc.* 34, 663–667 (2014).
4. Y.S. Sung, J.M. Kim, J.H. Cho, T.K. Song, M.H. Kim, H.H. Chong, T.G. Park, D. Do, and S.S. Kim, Effects of Na nonstoichiometry in $(Bi_{0.5}Na_{0.5+x})TiO_3$ ceramics. *Appl. Phys. Lett.* 96, 022901 (2010).
5. Y.S. Sung, J.M. Kim, J.H. Cho, T.K. Song, M.H. Kim, and T.G. Park, Effects of Bi nonstoichiometry in $(Bi_{0.5+x}Na)TiO_3$ ceramics. *Appl. Phys. Lett.* 98, 012902 (2011).
6. S. Tong, Y.E. von Schirnding, and T. Prapamontol, Environmental lead exposure: a public health problem of global dimensions. *Bull. World Health Organ.* 78, 1068–1077 (2000).
7. V.Q. Nguyen, H.S. Han, K.J. Kim, D.D. Dang, K.K. Ahn, and J.S. Lee, Strain enhancement in $Bi_{1/2}(Na_{0.82}K_{0.18})_{1/2}TiO_3$ lead-free electromechanical ceramics by co-doping with Li and Ta. *J. Alloys Compound.* 511, 237–241 (2012).
8. N.D. Quan, V.N. Hung, N.V. Quyet, H.V. Chung, and D.D. Dung, Band gap modification and ferroelectric properties of $Bi_{0.5}(Na, K)_{0.5}TiO_3$-based by Li substitution. *AIP Adv.* 4, 017122 (2014).
9. D.D. Dung, N.V. Quyet, and L.H. Bac, Role of Sintering Temperature on Giant Field-Induced Strain in Lead-Free $Bi_{0.5}(Na, K)_{0.5}TiO_3$-Based Ceramics. *Ferroelectrics* 474, 113–119 (2015).
10. N.V. Quyet, L.H. Bac, and D.D. Dung, Enhancement of the Electrical-field-induced Strain in Lead-free $Bi_{0.5}(Na, K)_{0.5}TiO_3$-based Piezoelectric Ceramics. *J. Korean Phys. Soc.* 66, 1317–1322 (2015).
11. L.H. Bac, H.S. Hong, D. Odkhuu, and D.D. Dung, Effect of sintering temperature on properties of lead-free piezoelectric $0975Bi_{05}(Na_{0.82}K_{0.18})_{05}TiO_3$-$0.025LiTaO_3$ ceramics. *J. Nanosci. Nanotech.* 16, 7929–7934 (2016).
12. L. Ju, C. Shi, L. Sun, Y. Zhang, H. Qin, and J. Hu, Room-temperature magnetoelectric coupling in nanocrystalline $Na_{0.5}Bi_{0.5}TiO_3$. *J. Appl. Phys.* 116, 083909 (2014).
13. N.A. Spaldin, and R. Ramesh, Advances in magnetoelectric multiferroics. *Nature Mater.* 18, 203–212 (2019).
14. Y. Zhang, J. Hu, F. Gao, H. Liu, and H. Qin, Ab initio calculation for vacancy-induced magnetism in ferroelectric $Na_{0.5}Bi_{0.5}TiO_3$. *Comput. Theor. Chem.* 967, 284–288 (2011).
15. D.D. Dung, N.T. Hung, and D. Odkhuu, Structure, optical and magnetic properties of new $Bi_{0.5}Na_{0.5}TiO_3$-$SrMnO_{3-\delta}$ solid solution materials. *Sci. Rep.* 9, 18186 (2019).
16. L.T.H. Thanh, N.B. Doan, N.Q. Dung, L.V. Cuong, L.H. Bac, N.A. Duc, P.Q. Bao, and D.D. Dung, Origin of room temperature ferromagnetism in Cr-doped lead-free ferroelectric $Bi_{0.5}Na_{0.5}TiO_3$ materials. *J. Electron. Mater.* 46, 3367–3372 (2017).
17. L.T.H. Thanh, N.B. Doan, L.H. Bac, D.V. Thiet, S. Cho, P.Q. Bao, and D.D. Dung, Making room-temperature ferromagnetism in lead-free ferroelectric $Bi_{0.5}Na_{0.5}TiO_3$ material. *Mater. Lett.* 186, 239–242 (2017).
18. D.D. Dung, N.B. Doan, N.Q. Dung, N.H. Linh, L.H. Bac, L.T.H. Thanh, N.N. Trung, N.V. Duc, L.V. Cuong, D.V. Thiet, and S. Cho, Tunable magnetism of $Na_{0.5}Bi_{0.5}TiO_3$ materials via Fe defects. *J. Supercond. Novel Magn.* 32, 3011–3018 (2019).
19. Y. Wang, G. Xu, L. Yang, Z. Ren, X. Wei, W. Weng, P. Du, G. Shen, G. Shen, and G. Han, Room-temperature ferromagnetism in Fe-doped $Na_{0.5}Bi_{0.5}TiO_3$ crystals. *Mater. Sci. Poland* 27, 471–476 (2009).
20. D.D. Dung, N.Q. Dung, N.B. Doan, N.H. Linh, L.H. Bac, N.N. Trung, N.V. Duc, L.T.H. Thanh, L.V. Cuong, D.V. Thiet, and S. Cho, Defect-mediated room temperature ferromagnetism in lead-free ferroelectric $Na_{0.5}Bi_{0.5}TiO_3$ materials. *J. Supercond. Novel Magn.* 33, 911–920 (2020).
21. Y. Wang, G. Xu, X. Ji, Z. Ren, W. Weng, P. Du, G. Shen, and G. Han, Room-temperature ferromagnetism of Co-doped $Na_{0.5}Bi_{0.5}TiO_3$. *J. Alloys Compound.* 475, L25–L30 (2009).
22. D.D. Dung, N.B. Doan, N.Q. Dung, L.H. Bac, N.H. Linh, L.T.H. Thanh, D.V. Thiet, N.N. Trung, N.C. Khang, T.V. Trung, and N.V. Duc, Role of Co dopants on the structural, optical and magnetic properties of lead-free ferroelectric $Na_{0.5}Bi_{0.5}TiO_3$ materials. *J. Sci. Adv. Mater. Dev.* 4, 584–590 (2019).
23. M.M. Hue, N.Q. Dung, L.T.K. Phuong, N.N. Trung, N.V. Duc, L.H. Bac, and D.D. Dung, Magnetic properties of (1–x) $Bi_{0.5}Na_{0.5}TiO_3$ + $xMnTiO_3$ materials. *J. Magn. Magn. Mater.* 471, 164–168 (2019).
24. M.M. Hue, N.Q. Dung, N.N. Trung, L.H. Bac, L.T.K. Phuong, N.V. Duc, and D.D. Dung, Tunable magnetic properties of $Bi_{0.5}Na_{0.5}TiO_3$ materials via solid solution of $NiTiO_3$. *Appl. Phys. A* 124, 588 (2018).
25. D.D. Dung, M.M. Hue, N.Q. Dung, N.H. Lam, L.T.K. Phuong, L.H. Bac, N.N. Trung, N.V. Duc, and D. Odkhuu, Enhancing room-temperature ferromagnetism in $Bi_{0.5}Na_{0.5}TiO_3$ via $FeTiO_3$ solid solution. *J. Electroceram.* 44, 129–135 (2020).
26. N.T. Hung, L.H. Bac, N.T. Hoang, P.V. Vinh, N.N. Trung, and D.D. Dung, Structural, optical, and magnetic properties of $SrFeO_{3-\delta}$-modified $Bi_{0.5}Na_{0.5}TiO_3$ materials. *Phys B Conden. Mater.* 531, 75–78 (2018).
27. N.T. Hung, L.H. Bac, N.N. Trung, N.T. Hoang, P.V. Vinh, and D.D. Dung, Room-temperature ferromagnetism in Fe-based perovskite solid solution in lead-free ferroelectric $Bi_{0.5}Na_{0.5}TiO_3$ materials. *J. Magn. Magn. Mater.* 451, 183–186 (2018).
28. D.D. Dung, N.T. Hung, and D. Odkhuu, Magnetic and optical properties of $MgMnO_{3-\delta}$-modified $Bi_{0.5}Na_{0.5}TiO_3$ materials. *J. Magn. Magn. Mater.* 482, 31–37 (2019).
29. D.D. Dung, N.T. Hung, and D. Odkhuu, Magnetic and optical properties of new (1–x) $Bi_{0.5}Na_{0.5}TiO_3$ + $xBaMnO_{3-\delta}$ solid solution materials. *Appl. Phys. A* 125, 465 (2019).
30. D.D. Dung, and N.T. Hung, Structural, optical, and magnetic properties of the new $(1–x)Bi_{0.5}Na_{0.5}TiO_3$ + $xMgCoO_{3-\delta}$ solid solution system. *J. Supercond. Nov. Magn.* 33, 1249–1256 (2020).
31. D.D. Dung, and N.T. Hung, Magnetic properties of (1–x) $Bi_{0.5}Na_{0.5}TiO_3$ + $xSrCoO_{3-\delta}$ solid-solution materials. *Appl. Phys. A* 126, 240 (2020).
32. N.T. Hung, N.H. Lam, A.D. Nguyen, L.H. Bac, N.N. Trung, D.D. Dung, Y. Kim, N. Tsogbadrakh, T. Ochirkhuyag, and D. Odkhuu, Intrinsic and tunable ferromagnetism in $Bi_{0.5}Na_{0.5}TiO_3$ through $CaFeO_{3-\delta}$ modification. *Sci. Rep.* 10, 6189 (2020).
33. D.D. Dung, N.H. Lam, A.D. Nguyen, N.N. Trung, N.V. Duc, N.T. Hung, Y.S. Kim, and D. Odkhuu, Experimental and theoretical studies on induced ferromagnetism of new $(1–x)Na_{0.5}Bi_{0.5}TiO_3$ + $xBaFeO_{3-\delta}$ solid solution. *Sci. Rep.* 11, 8908 (2021).
34. D.D. Dung, N.T. Hung, and D. Odkhuu, Magnetic and optical properties of new $(1–x)Bi_{0.5}Na_{0.5}TiO_3$+$xCaMnO_{3-\delta}$ solid solution materials. *Mater. Sci. Eng. B* 263, 114902 (2021).

35. D.D. Dung, and N.T. Hung, Magnetic properties of (1–x) $Bi_{0.5}Na_{0.5}TiO_3$ + x$CaCoO_{3-\delta}$ solid-solution system. *J. Electron. Mater.* 49, 5317–5325 (2020).
36. D.D. Dung, and N.T. Hung, Structural, optical and magnetic properties of (1–x)$Bi_{0.5}Na_{0.5}TiO_3$+x$BaCoO_{3-\delta}$ solid solution systems prepared by the sol-gel method. *J. Nanosci. Nanotech.* 21, 2604–2612 (2021).
37. D.D. Dung, M.M. Hue, N.Q. Dung, L.T.K. Phuong, L.H. Bac, N.X. Duong, P.D. Luong, N.A. Duc, N.N. Trung, N.H. Thoan, and D. Odkhuu, Influenced of $Bi(Ti_{1/2}Ni_{1/2})O_3$ concentration on the structural, optical and magnetic properties of lead-free $Bi_{1/2}Na_{1/2}TiO_3$ materials. *Vacuum* 177, 109306 (2020).
38. The Materials Project. Materials Data on $Ca_2Ni_2O_5$ by Materials Project. United States: N. p., 2020. Web. https://doi.org/10.17188/1320817.
39. The Materials Project. Materials Data on $CaNiO_3$ by Materials Project. United States: N. p., 2020. Web. https://doi.org/10.17188/1320823.
40. The Materials Project. Materials Data on $CaNiO_2$ by Materials Project. United States: N. p., 2014. Web.https://doi.org/10.17188/1320329.
41. S. Singh, S.K. Srivastav, A. Patel, A. Kumar, R. Chatterjee, T. Takeuchi, and S.K. Pandey, Enhancement in thermoelectric properties of n-type $(La_{0.7}Sr_{0.3}MnO_3)_{0.5}$ $(NiO)_{0.5}$: composite and nanostructure effect. *J. Phys. D: Appl. Phys.* 55, 065503 (2022).
42. L.T.H. Thanh, N.H. Tuan, L.H. Bac, D.D. Dung, and P.Q. Bao, Influence of growth condition on the microstructural, phase stability and optical properties of lead-free ferroelectric $Bi_{0.5}Na_{0.5}TiO_3$ materials. *Commun. Phys.* 26, 51–57 (2016).
43. R.D. Shannon, Revised effective ionic radii and systematic studies of interatomic distances in halides and chalcogenides. *Acta Cryst. A* 32, 751–767 (1976).
44. S.K. Pradhan, and S.K. De, Dielectric and optical properties of Ni doped $Na_{0.5}Bi_{0.5}TiO_3$. *Ceram. Int.* 44, 15181–15191 (2018).
45. C. Chatzichristodoulou, P. Norby, P.V. Hendriksen, and M.B. Mogensen, Size of oxide vacancies in fluorite and perovskite structured oxides. *J. Electroceram.* 34, 100–107 (2015).
46. M. Naderer, T. Kainz, D. Schutz, and K. Reichmann, The infuclence of Ti-nonstoichiometry in $Bi_{0.5}Na_{0.5}TiO_3$. *J. European Ceram. Soc.* 34, 663–667 (2014).
47. M. Spreitzer, M. Valant, and D. Suvorov, Sodium deficiency in $Na_{0.5}Bi_{0.5}TiO_3$. *J. Mater. Chem.* 17, 185–192 (2007).
48. I.K. Jeong, Y.S. Sung, T.K. Song, M.H. Kim, and A. Llobet, Structural evolution of bismuth sodium titanate induced by *A*-site non-stoichiometry: Neutron powder diffraction studies. *J. Korean Phys. Soc.* 67, 1583–1587 (2015).
49. X. Liu, H. Fan, J. Shi, L. Wang, and H. Du, Enhanced ionic conductivity of Ag addition in acceptor-doped $Bi_{0.5}Na_{0.5}TiO_3$ ferroelectrics. *RSC Adv.* 6, 30623–30627 (2016).
50. M.K. Niranjan, T. Karthik, S. Asthana, J. Pan, and U.V. Waghmare, Theoretical and experimental investigation of raman modes, ferroelectric and dielectric properties of relaxor $Na_{1/2}Bi_{1/2}TiO_3$. *J. Appl. Phys.* 113, 194106 (2013).
51. N.H. Linh, N.H. Tuan, D.D. Dung, P.Q. Bao, B.T. Cong, and L.T.H. Thanh, Alkali metal-substituted bismuth-based perovskite compounds: a DFT study. *J. Sci. Adv. Mater. Dev.* 4, 492–498 (2019).
52. D.D. Dung, D.V. Thiet, D.A. Tuan, and S. Cho, Strain effects in epitaxial Mn_2O_3 thin film grown on MgO(100). *J. Appl. Phys.* 113, 17A314 (2013).
53. Y. Lin, C.W. Nan, J. Wang, H. He, J. Zhai, and L. Jiang, Photoluminescence of nanosized $Na_{0.5}Bi_{0.5}TiO_3$ synthesized by a sol–gel process. *Mater. Lett.* 58, 829–832 (2004).
54. N.H. Tuan, L.H. Bac, L.V. Cuong, D.V. Thiet, T.V. Tam, and D.D. Dung, Structural, optical, and magnetic properties of lead-free ferroelectric $Bi_{0.5}K_{0.5}TiO_3$ solid solution with $BiFeO_3$ materials. *J. Electron. Mater.* 46, 3472–3478 (2017).
55. J.M.D. Coey, A.P. Douvalis, C.B. Fitzgerald, and M. Venkatesan, Ferromagnetism in Fe-doped SnO_2 thin films. *Appl. Phys. Lett.* 84, 13332 (2004).
56. S.J. Clark, M.D. Segall, C.J. Pickard, P.J. Hasnip, M.J. Probert, K. Refson, and M.C. Payne, First principles methods using CASTEP. *Z. Kristallogr.* 220, 567–570 (2005).
57. J.P. Perdew, K. Burke, and M. Ernzerhof, Generalized Gradient Approximation Made Simple. *Phys. Rev. Lett.* 77, 3865 (1996).
58. H.J. Monkhorst, and J.D. Pack, Special points for Brillouin-zone integrations. *Phys. Rev. B* 13, 5188 (1976).
59. J. Padilla, and D. Vanderbilt, Ab-initio study of $BaTiO_3$ surfaces. *Phys. Rev. B* 56, 1625 (1997).
60. D.D. Dung, N.Q. Dung, M.M. Hue, N.H. Lam, L.H. Bac, L.T.K. Phuong, N.N. Trung, D.D. Tuan, N.D. Quan, D. Sangaa, and D. Odkhuu, Experimental and theoretical studies on the room-temperature ferromagnetism in new (1–x)$Bi_{1/2}Na_{1/2}TiO_3$+x$CoTiO_3$ solid solution materials. *Vacuum* 179, 109551 (2020).
61. J. Goldsby, S. Raj, S. Guruswamy, and D.D. Azbill, First-principle and experimental study of a gadolinium-praseodymium-cobalt pseudobinary intermetallic compound. *J. Mater.* 2015, 753612 (2015).

Publisher's Note Springer Nature remains neutral with regard to jurisdictional claims in published maps and institutional affiliations.